



**HAL**  
open science

## **3D Analysis of Helium-3 Nanobubbles in Palladium Aged under Tritium by Electron Tomography**

Bérengère Evin, Éric Leroy, Walid Baaziz, Mathieu Segard, Valérie Paul-boncour, Sylvain Challet, Arnaud Fabre, Stéphanie Thiébaud, Michel Latroche, Ovidiu Ersen

► **To cite this version:**

Bérengère Evin, Éric Leroy, Walid Baaziz, Mathieu Segard, Valérie Paul-boncour, et al.. 3D Analysis of Helium-3 Nanobubbles in Palladium Aged under Tritium by Electron Tomography. *Journal of Physical Chemistry C*, 2021, 125 (46), pp.25404–25409. 10.1021/acs.jpcc.1c07906 . hal-03460741

**HAL Id: hal-03460741**

**<https://hal.science/hal-03460741>**

Submitted on 1 Dec 2021

**HAL** is a multi-disciplinary open access archive for the deposit and dissemination of scientific research documents, whether they are published or not. The documents may come from teaching and research institutions in France or abroad, or from public or private research centers.

L'archive ouverte pluridisciplinaire **HAL**, est destinée au dépôt et à la diffusion de documents scientifiques de niveau recherche, publiés ou non, émanant des établissements d'enseignement et de recherche français ou étrangers, des laboratoires publics ou privés.

# 3D Analysis of Helium-3 Nanobubbles in Palladium Aged under Tritium by Electron Tomography

## *AUTHOR NAMES*

*Bérengère Evin<sup>1\*‡</sup>, Éric Leroy<sup>2‡</sup>, Walid Baaziz<sup>3‡</sup>, Mathieu Segard<sup>1‡</sup>, Valérie Paul-Boncour<sup>2‡</sup>,  
Sylvain Challet<sup>1‡</sup>, Arnaud Fabre<sup>1‡</sup>, Stéphanie Thiébaud<sup>1‡</sup>, Michel Latroche<sup>2‡</sup>, Ovidiu Ersen<sup>3‡</sup>*

## *AUTHOR ADDRESS*

<sup>1</sup> CEA, DAM, Valduc, F-21120, Is-sur-Tille, France

<sup>2</sup> Univ Paris-Est Creteil, CNRS, ICMPE (UMR 7182), 2 rue Henri Dunant, F-94320 Thiais,  
France

<sup>3</sup> Institut de Physique et Chimie des Matériaux de Strasbourg, CNRS, UMR 7504, 23 rue du  
Loess 67034 Strasbourg, France

## *KEYWORDS*

*Electron tomography, Nanobubbles, Palladium tritide, Distances*

## *ABSTRACT*

A 3D analysis at the nanoscale has been used to characterize helium-3 nanobubbles in palladium powders aged several years under tritium for assessing their structural characteristics and spatial

distribution. These helium-3 nanobubbles are formed by tritium radioactive decay and exhibit diameters centered around 2.5 nm. Scanning transmission electron microscopy (STEM) has been used to acquire tomographic series on typical zones of the macroscopic specimen containing helium nanobubbles. Electron tomography data treatments have been achieved allowing 3D structural analysis of helium-3 nanobubbles. For the first time, inter-distances between bubbles have been determined with a mean value between 8 and 10 nm. The swelling of the aged material varies between 8 and 18% in agreement with macroscopic measurements and modeling.

## INTRODUCTION

Palladium and its alloys can be used as tritium solid-state storage materials by forming tritides. However, upon time, tritium radioactive decay ( $t_{1/2}=12.3$  years) produces helium-3 that is not soluble in palladium. Helium-3 atoms diffuse and gather to form nanobubbles that modify the physical and thermodynamic properties of palladium tritide. This phenomenon is commonly called the "aging process". Here the aging process is divided in three steps: bubbles nucleation, growth and accelerated helium desorption. The bubble nucleation modeling involves a cellular automaton<sup>1</sup> describing the material at the atomic scale and considers the physical phenomena involved in the bubble nucleation, namely tritium diffusion, formation of helium-3 by radioactive tritium decay, helium-3 diffusion and also helium-3 self-trapping. This modeling has shown that the spatial repartition of helium bubbles is set during the first months of aging<sup>1</sup>. In fact, when the number of bubbles generated is large enough, a new isolated helium-3 atom has a greater probability to meet an existing bubble than other isolated atoms during its diffusion to create a new bubble. These calculations lead to a log-normal distribution of bubble spacing with a maximum close to 5 nm (depending on the helium diffusion coefficient)<sup>1</sup>. Measuring the distances between bubbles will

allow us to remove the uncertainty on this data, improve the reliability of the automaton and made better predictions on the aging process. The bubble growth is modeled using a continuum mechanics calculation <sup>2</sup>. Bubble size, pressure and material swelling are the output parameters. Bubble size <sup>3</sup> and pressure <sup>4</sup> are measured by TEM and STEM-EELS. Measuring material swelling will improve the reliability of the model.

Palladium-based materials aging has been studied at several scales including the microscopic one <sup>3</sup>. Indeed, microstructure and pressure of helium-3 nanobubbles can provide valuable information on the aging process and help its modeling. Helium-3 nanobubbles size and density have already been determined by TEM (Transmission Electron Microscopy) in palladium powders aged under tritium <sup>3</sup> and in other materials such as erbium tritide <sup>5</sup> or uranium oxide <sup>6</sup>. In addition, helium-3 density (bubble pressure) in those nanobubbles has been measured using EELS spectroscopy (Electron Energy-Loss Spectroscopy) in palladium <sup>4</sup> and in palladium alloys <sup>7</sup>. All those microscopic studies have been very useful leading to a better understanding of the aging process and enhancing the modeling of this phenomenon <sup>1</sup>.

However, since classical TEM imaging gives only a 2D projected information, those previous studies have provided two-dimensional parameters that do not reflect the 3D distribution of helium-3 nanobubbles. From 2D TEM experiments, the helium-3 bubbles exhibit diameters centered around 2.5 nm <sup>3</sup>. From the material perspective, the analysis of the 3D spatial distribution of these cavities should provide the distances between the helium-3 bubbles and the material swelling, which are key parameters for the aging process modeling and could not be obtained by classical TEM.

Electron tomography allows to study the 3D microstructure of low-Z inclusions in dense matrix <sup>8</sup>. This technique has also been applied to needles of aged palladium alloys <sup>9</sup>. To provide reliable three-dimensional parameters on palladium powders aged under tritium, electron tomography technique has also been used in this work. This technique consists in the acquisition of 2D images of the sample at different tilt angles ( $\pm 70^\circ$ ). Then, a backprojection-based algorithm may be used to calculate the 3D volume of the original sample. From the methodological point of view, the goal here is to investigate the feasibility of the tomography measurement on those powder samples characterized by the presence of nanoscale low-Z inclusions in a denser matrix.

In this article, we report on the tomography study on three palladium powders samples aged several years under tritium. Post-processing of the 3D data acquisition has been performed with a special attention for the analysis of these cavities.

## EXPERIMENTAL CONDITIONS

The acquisitions were performed for three different palladium samples aged under tritium between 5 and 8.5 years in powder form. The synthesis of palladium tritide powders and the decontamination process are described in a previous work <sup>10</sup>.

Powders were embedded in an epoxy resin. TEM samples were cut using ultramicrotomy at room temperature with a diamond knife and deposited on a 400 mesh copper grid. Before tomography measurement, the sample surface was cleaned in an Ar/H<sub>2</sub> plasma to remove the carbonated contamination.

The tilt series electron tomography acquisition was performed with a JEOL 2100F probe-corrected operated at 200kV in STEM mode (Scanning Transmission Electron Microscope). The detectors

configuration allows to acquire both HAADF (High Angle Annular Dark Field) and BF (Bright Field) images. Camera length is 10 cm, the collection angles of the HAADF detector are 60 mrad (internal) and 120 mrad (external) and the convergence angle is 20 mrad (with a 30  $\mu\text{m}$  condenser diaphragm). Typical tomography acquisition was done at room temperature between  $-65/+70^\circ$  with a  $2^\circ$  step. It is necessary to consider the low stability of the sample under the electron beam. The  $2^\circ$  step lowers the number of acquired images, which impacts final resolution. However, the elongation induced by the tilt step is small. Indeed, using the Crowther criterion<sup>11</sup>, for a 1 nm bubble, the elongation along the Z axis is less than 0.07 nm, which is far lower than the pixel size since the spatial resolution in the 2D-STEM images is between 0.22 and 0.55 nm.

Finally, a drop of a solution of nano-gold beads (5 nm diameter) was deposited on the grid of the microscopy sample to ease post-processing of the data, in particular the alignment protocol of the projection images belonging to the same tilt series.

## DATA PROCESSING

Post-treatment of the tomographic tilt series consists of three steps: i) alignment of the tomography images, ii) reconstruction of a 3D volume and, iii) segmentation. Data treatment is performed using TomoJ<sup>12</sup>, an ImageJ plugin<sup>13,14</sup> for the 3D reconstruction, and Slicer<sup>15</sup> for the visualization. The post-processing treatments were performed using the same parameters for all acquisitions.

After a rough alignment using a cross-correlation algorithm, the tilt series alignment was improved by considering the positions of gold nanoparticles as fiducial markers.

The reconstruction has been calculated using ART algorithm (Algebraic Reconstruction Technique). The number of iterations was 100 and the relaxation parameter was set to 0.01. With the use of a GPU (Graphics Processing Unit), the calculation lasts only few minutes. The

reconstruction is often cropped in (X, Y, Z) directions in order to reduce calculation time for segmentation.

The last step of the post-processing is the segmentation consisting in selecting pixels using pre-defined criteria, based principally on their gray-level intensities. In our case, the goal is to isolate helium-3 bubbles. Isolating cavities from the palladium matrix is easily achieved since the cavities appear as black pixels and palladium as light grey. However, it is not possible to isolate cavities from background directly since their grey levels are very close. To isolate the cavities, the reconstruction was filtered applying 3D Gaussian or median filter (2 pixels' radius)<sup>16</sup> and the dark background was removed using the rolling ball algorithm of ImageJ with a 30 pixels' radius<sup>17</sup>.

The background-less reconstruction is thresholded to extract cavities. At this stage, a mask of the cavities is obtained, it can be manually corrected to improve the result. This mask is converted into a 3D volume using Slicer software. The same steps are followed to obtain 3D volume of the palladium grain.

## RESULTS

Figure 1 shows the STEM images at 0° tilt extracted from the tilt series acquired by electron tomography for palladium sample aged during 5 years under tritium. Some cavities are circled in red.

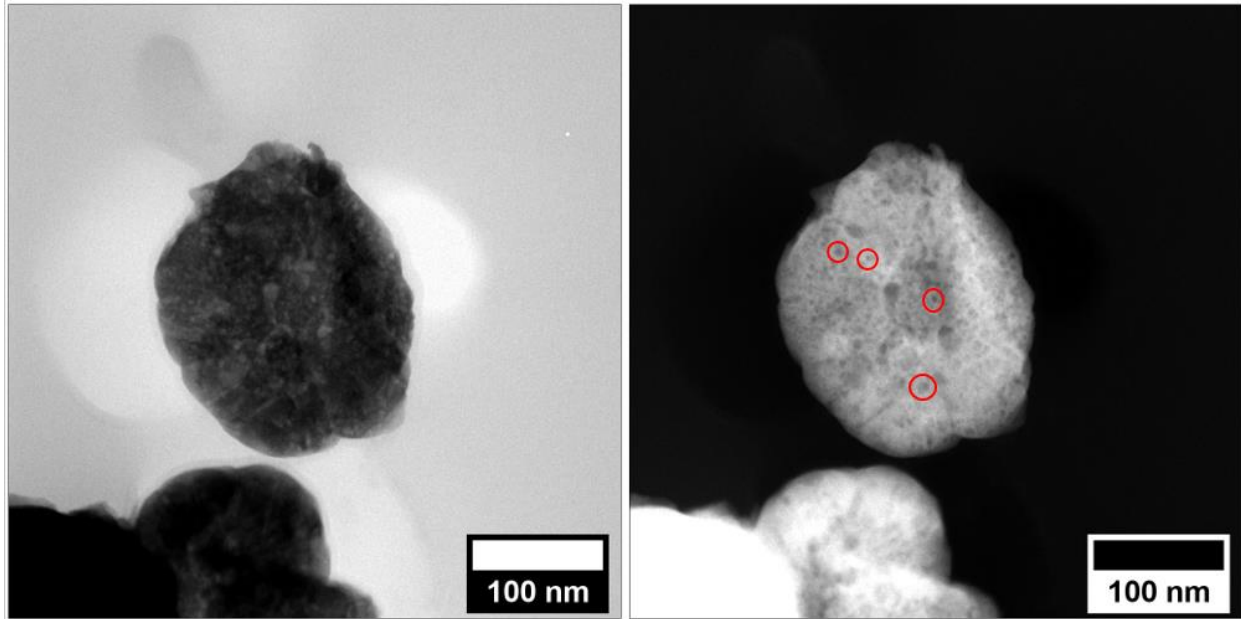


**Figure 1** – Bright Field (left) and High Angle Annular Dark Field (right) images at  $0^\circ$  tilt from the electron tomography series of palladium sample aged under tritium during five years. The pixel size is 0.45 nm. The image size is 1024x1024 in pixel unit.

Cavities can be easily observed as white spots on the BF (Bright Field) image (left) and as dark holes on the HAADF image (right). The high spatial resolution allows to clearly visualize cavities with nanometric sizes.

Due to low Z contrast of helium, the tomography measurements do not allow to identify whether the cavities are filled with helium or empty. Such information can be obtained by EELS as demonstrated in a previous study <sup>4</sup>. In this previous work, it was shown that some helium nanobubbles are in fact empty cavities. However, empty cavities have the same microstructure than helium bubbles, because they were probably initially filled with He, which has desorbed during the sample preparation or under beam irradiation. In the present study, « nanobubble » will therefore refers to any cavity filled or not with helium-3.

Figure 2 shows one of the projection images from the initial tilt series (left) and a typical slice through the calculated reconstruction (right) for a palladium sample aged 8.5 years under tritium. Some cavities are circled in red.

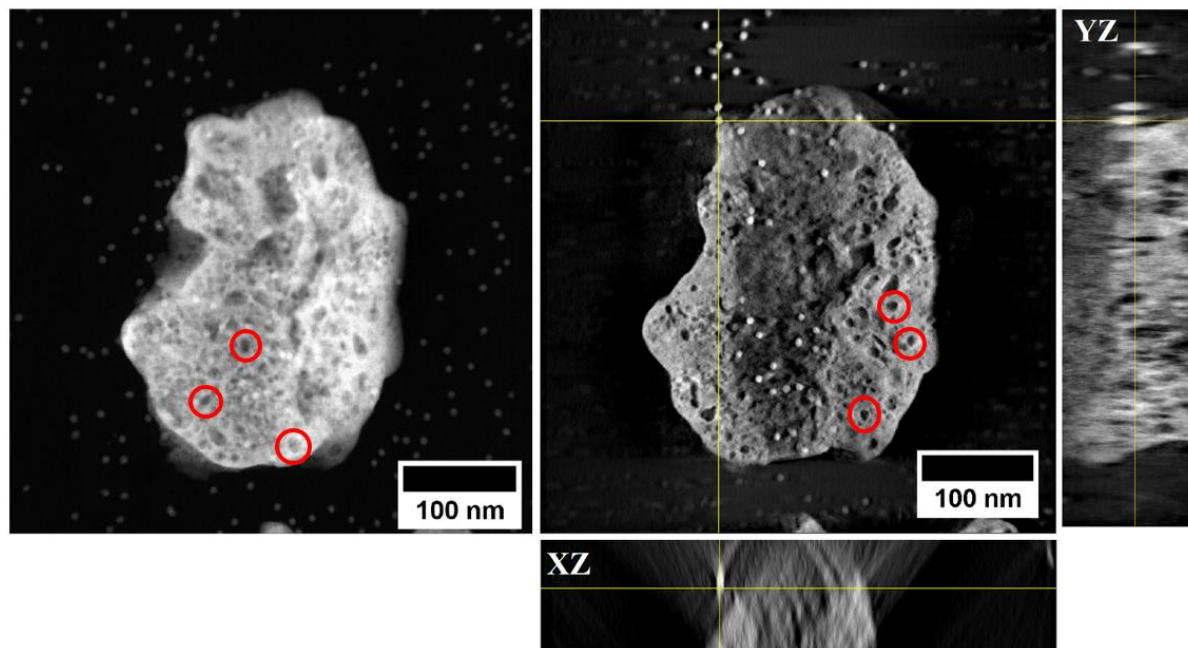


**Figure 2** – One of the HAADF images from the corresponding tilt series acquired, the tilting angles are  $-64^\circ$  and  $+60^\circ$  with a  $2^\circ$  increment (left) and a typical (X,Y) slice through the calculated reconstruction (right) and the associated (X,Z) and (Y,Z) projections for palladium powder aged 8.5 years under tritium. The size of the image is 1024x1024 in pixel unit and the pixel size is 0.45 nm.

In Figure 2 the gold nanoparticles can be unambiguously assigned to the little light spots on the black background (left). Once the reconstruction is calculated, its accuracy can be visually checked by analyzing the shape of the gold nanoparticles in the reconstruction visualized in cross section, with the basic rule that " the calculated reconstruction of an object having a spherical shape in all the 2D projections should be a sphere ". The gold nanoparticles are slightly elongated in the (Y,Z) (X,Z) projections due to the missing wedge but keep a spherical shape. Regarding now the analyzed grain and its features of interest, we can observe that the helium-3 nanobubbles are mostly spherical and remarkably distinct in the reconstruction, delimited by well-defined contours.

The reconstruction is then thresholded to isolate helium-3 bubbles and palladium grain. Figure 3 illustrates this processing step by directly comparing the views of the calculated reconstruction (left) and the 3D model of the grain obtained by segmentation (right). Some cavities are circled in red.

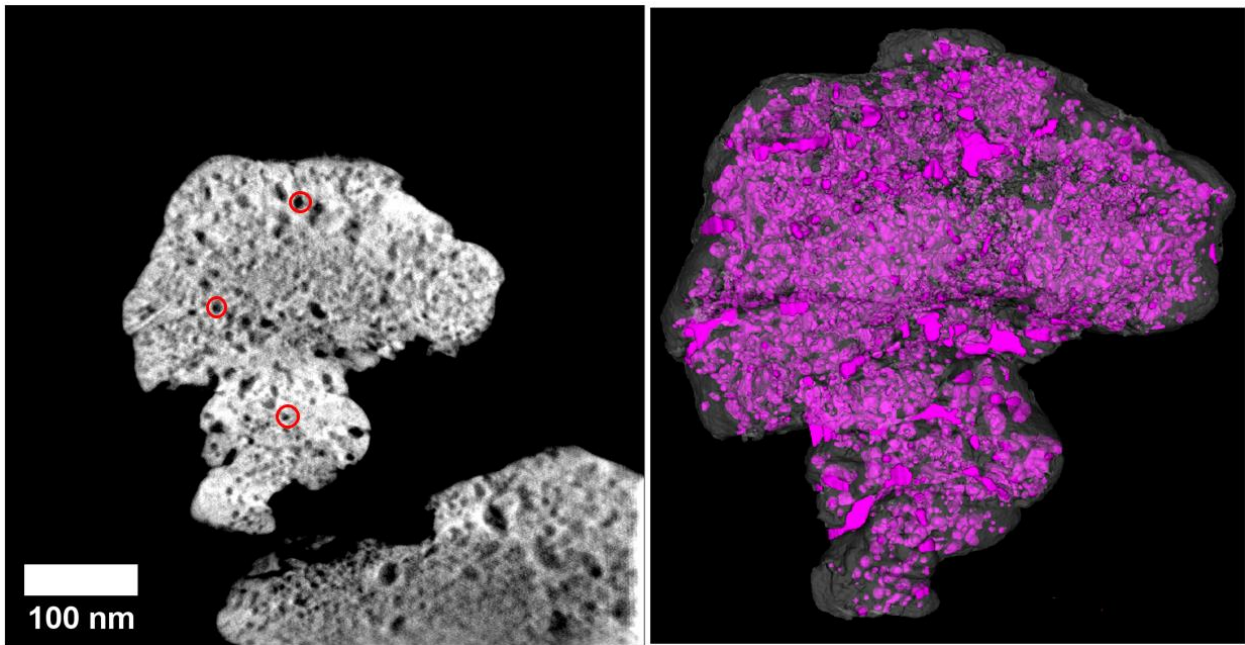


**Figure 3** – Typical slice through the reconstruction (left) and the segmentation (right) of a palladium particle aged 6.5 years under tritium. For this tomography the tilting angles are between  $-78^\circ$  and  $+68^\circ$ . The size of the image is  $667 \times 737$  in pixel unit and the pixel size is 0.55 nm.

In the segmentation, the cavities are represented in pink and the palladium grain in grey. More cavities can be seen on the segmentation image since in this case all the grain volume is represented whereas just one slice is shown on the left image extracted from the reconstruction.

## DATA QUANTIFICATION

As mentioned previously, the 3D models of the cavities and the palladium grain are extracted using cavities and palladium masks and subsequently quantified with the function "3D Manager" available in the ImageJ software<sup>16</sup>. This function gives access to the cavities surface, volume, and

coordinates. Cavities density is calculated using the number of cavities and the grain volume given by 3D Manager function <sup>16</sup> of ImageJ software. Figure 4 presents the cavities diameters obtained by analyzing the corresponding 3D models for the three studied samples.

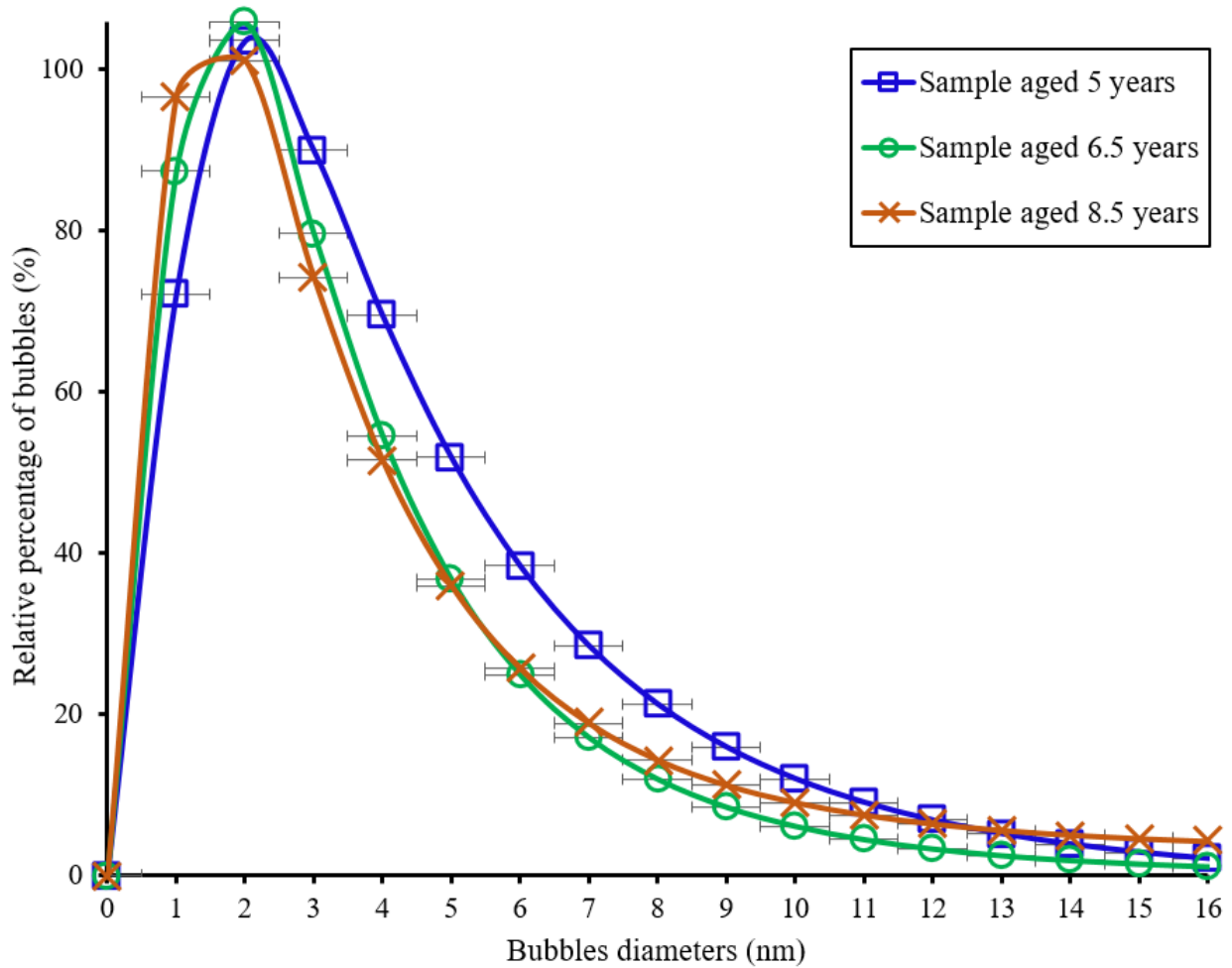


**Figure 4** – Log-normal fitting of helium-3 bubbles diameters distribution obtained from the quantitative analysis of the 3D models obtained by electron tomography on representative grains of the three studied samples of palladium aged 5 (blue square), 6.5 (green circle) and 8.5 (orange cross) years under tritium.

For the three samples aged 5 years, 6.5 and 8.5 years the bubbles diameters distribution yields a maximum at 2.0 ( $\pm 1$ ) nm. All the cavities size distributions follow a log-normal type function. It is remarkable the three samples have close bubbles sizes, which confirms that after several years the bubble size evolution is stabilized as predicted by the modeling. The bubble size measurement

is in agreement with previous 2D-TEM study<sup>3</sup> and validates the mechanical modeling of bubble growth<sup>2</sup>.

A homemade script (see Supplementary Materials) calculates the first-neighbor distance from cavities center coordinates. Figure 5 represents the fitting of the histogram of the in-between distances of cavities center to center for the three studied samples. The size and distribution are in the expected order of magnitude<sup>3</sup>.

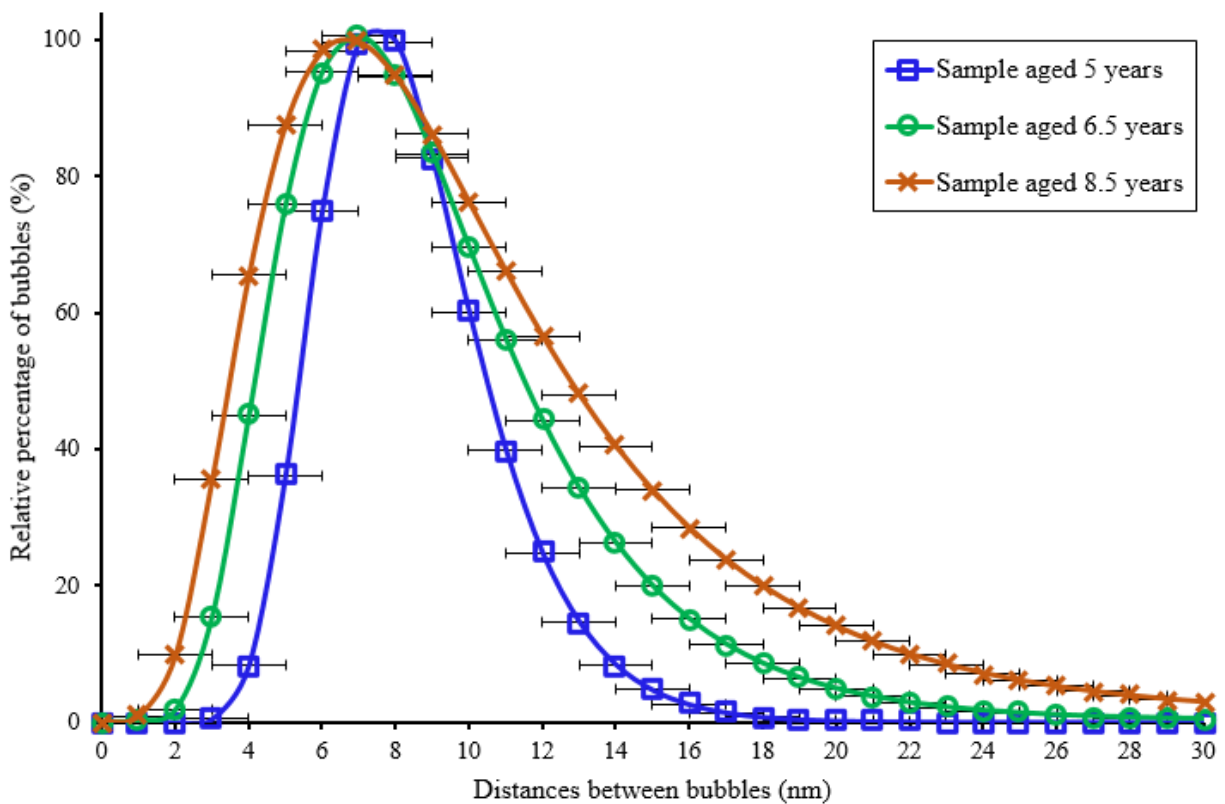


**Figure 5** – Log-normal fitting of distances between helium-3 bubbles, center-to-center, for the three studied samples of palladium aged 5 (blue square), 6.5 (green circle) and 8.5 (orange cross) years under tritium. The distances have been obtained by analyzing the positions of all the cavities from the considered grain as deduced by electron tomography.

It is worth noticing that, despite the difference in aging time, the distances between cavities are quite similar for the three samples. Only a small broadening of the distances distributions is

observed between the three samples which could be attributed to the appearance of a slight heterogeneity with aging. This is consistent with the fact that the density of bubbles, so 3D repartition, is fixed during the first months of aging and do not evolve much after <sup>1</sup>. As told in the introduction part, when the number of bubbles generated is large enough, a new isolated helium-3 atom has a greater probability to enter a bubble than create a new one. And even if the time to reach this steady state depends on helium mobility, all calculations lead to months timescales to get it. Self-trapping mechanism, modeled in the cellular automaton <sup>1</sup>, predicts a log-normal distribution for the bubble distances. This tendency is confirmed by tomography measurements which also validates the bubble-spacing predictions of the automaton.

For the first time, using tomography, the distances between nanobubbles in palladium powders aged several years under tritium have been determined. The distributions of the first-neighbor distances between bubbles are maximum between 8 ( $\pm 1$ ) and 10 ( $\pm 1$ ) nm.

Cavities to palladium grain volumes ratios have also been measured and are 8% (5 years), 18% (6.5 years) and 18% (8.5 years). This parameter is important because it characterizes the swelling of the materials as the quantity of helium generated by tritium decay increases and is more sensitive to aging time than the mean bubble size diameter. To determine whether tomography, performed on only few grains, yields quantitative results, we have compared these data with those obtained on few grams of powders – typically from 1 to 2 g – by pycnometry measurements (Quantachrome Ultrapvc 1200e with helium-4 gas), which allow to follow the macroscopic evolution of the density. The swelling measured by pycnometry on palladium powders aged under tritium is 15% (5 years), 19% (6.5 years) and 22 % (8.5 years). The slight difference observed between both methods for the younger sample (8% versus 15%) will be further investigated. Assuming that the swelling is mainly induced by helium-3 bubbles <sup>2</sup> growth, tomography and pycnometry provide

results that are in excellent agreement. This last comparison validates the results of tomography to be quantitative information for all samples since the microscopic swelling quantification is consistent with the macroscopic one performed by pycnometry and can be used for the study of further samples. Moreover, these values are in good agreement with the one predicted by the mechanical modeling of the helium bubble growth <sup>2</sup>.

## BENEFIT OF THE TOMOGRAPHY ANALYSIS

Previous TEM study revealed that cavities exhibit dispersed diameters from 1 to 20 nm but are mainly centered around 2.5 nm <sup>3</sup>. Cavity densities, determined using TEM, are around  $4.10^{23}$  cavity/m<sup>3</sup> and helium-3 density in bubbles was measured around 70 He/nm<sup>3</sup> using EELS spectroscopy <sup>4</sup>. TEM <sup>3</sup> and tomography analysis give access to microstructural information of the cavities. The helium-3 filling of the cavities is studied by STEM-EELS <sup>4</sup> which allow to confirm the presence of helium-3 nanobubbles. Regarding the electron tomography analysis, in addition to cavities distances which can be measured only by such a 3D analysis, the size and density of cavities have been unambiguously measured using tomography data. Indeed, tomography gives access to the volume which eliminates the uncertainty of grain volume measurement when doing 2D TEM imaging. Even considering the effect of both the missing wedge and the tilt step, the Crowther's criterion<sup>11</sup> gives an elongation for a 1 nm bubble of less than 0.07 nm along the Z axis, a largely satisfactory accuracy for such experiments.

Nanobubbles median diameter measured using electron tomography is around 2.0 nm and the cavities density is between  $1.10^{23}$  and  $5.10^{23}$  cavity/m<sup>3</sup>. Cavity size is slightly lower and cavity density is a little lower than TEM results <sup>3</sup>. This can be explained by the small size of cavities and the 3D data processing steps, in particular the data segmentation. In fact, some of the smallest

cavities are hardly separated during the segmentation step, due to the small number of pixels they contain, which finally increases the mean size and lower the density. On the other hand, due to the redundancy of information provided by the use of several images in the data processing protocol, the electron tomography analysis allows to distinguish in the calculated reconstruction (before any segmentation step), small cavities which are in principle not visible in a classical 2D image. Ultimately electron tomography provides results that are consistent with the earlier TEM.

All these microstructural data are needed to model the aging process. The first aging step, nucleation, is modeled by a self-trapping mechanism using a cellular automaton <sup>1</sup>. For this calculation, bubble spacing and density are key parameters. The second step, bubble growth, is modeled by a continuum mechanics calculation <sup>2</sup>. This model uses the bubble size, density, material swelling and mechanical characteristics. The microstructural data acquired by tomography are consistent with the modeling predictions and therefore validate the mechanisms and models that have been used. For the last aging step, which occurs beyond 10 years, further experimental data are expected to clearly establish the mechanism responsible for accelerated helium release: bubble percolation, material fracture or helium diffusion.

## CONCLUSION

In conclusion, the present study of helium-3 nanobubbles microstructure demonstrates the suitability of electron tomography to analyze the microstructural properties of palladium powders aged several years under tritium.

Tomography treatments have been completed and yield 3D microstructural analysis of helium-3 nanobubbles generated in aged palladium tritide. Combined with a customized protocol for the quantification of the 3D data, it gives access to original parameters such as the distance between

cavities (assigned to the first neighbor distance in the 3D spatial arrangement of the cavities) or the cavity to grain volume ratio (material swelling).

Some other more conventional parameters (the mean size and the density of the cavities) are also measured and are in agreement with previous 2D TEM study. All in all, the two types of results are in good agreement, with an additional benefit for the electron tomography given by the possibility to calculate the distances between cavities and the swelling of the sample. The results highlight the relevance of electron tomography for the structural characterization of helium-3 nanobubbles in palladium aged under tritium.

The as obtained data allow to improve the understanding and the subsequent modeling of the aging process. The theoretical predictions of the cellular automaton (nucleation step) and of the mechanical model (growth step) agree with the tomography findings, which validates the relevance and reliability of self-trapping and mechanical mechanisms. The suitability of electron tomography on palladium powders aged under tritium opens new perspectives for a more detailed analysis of samples with different aging time to be able to better characterize the evolution of the 3D microstructural parameters over time.

## AUTHOR INFORMATION

### **Corresponding Author**

\* Bérengère Evin (berengere.evin@icmpe.cnrs.fr ; berengere.evin@protonmail.com )

Phone number : (+33) 149781214

Postal adress : ICMPE-CNRS, 2-4 rue Henri Dunant, 94320 Thiais, France

### **Author Contributions**

The manuscript was written through contributions of all authors. All authors have given approval to the final version of the manuscript. ‡These authors contributed equally.

## Funding Sources

This work was supported by the France's Atomic Energy Commission (C.E.A.) and by the French National Center for Scientific Research (C.N.R.S.).

## Supporting Information

Illustration of the post-processing steps for a tomography acquisition of the palladium powder aged 8.5 years under tritium – Homemade script written in Fortran to calculate the distances between bubbles.

## Acknowledgment

The authors acknowledge financial support from the CNRS-CEA “METSA” French network (FR CNRS 3507) on the TEM platform of IPCMS.

## REFERENCES

- (1) Segard, M.; Fabre, A.; Thiébaud, S.; Montheillet, F. Bubble Nucleation Process in a Metal Tritide Modeled Using a Cellular Automaton. *J. Nucl. Mater.* **2012**, *420* (1), 388–395. <https://doi.org/10.1016/j.jnucmat.2011.10.014>.
- (2) Montheillet, F.; Delaplanche, D.; Fabre, A.; Munier, E.; Thiébaud, S. A Mechanical Analysis of Metallic Tritide Aging by Helium Bubble Growth. *Mater. Sci. Eng. A* **2008**, *494* (1), 407–415. <https://doi.org/10.1016/j.msea.2008.04.033>.
- (3) Segard, M.; Leroy, E.; Evin, B.; Thiebaud, S.; Fabre, A.; Challet, S.; Paul-Boncour, V. TEM Observations on Palladium Samples Aged up to 8 Years under Tritium. *ArXiv210601776 Cond-Mat* **2021**.
- (4) Evin, B.; Leroy, E.; Segard, M.; Paul-Boncour, V.; Challet, S.; Fabre, A.; Latroche, M. Investigation by STEM-EELS of Helium Density in Nanobubbles Formed in Aged Palladium Tritides. *J. Alloys Compd.* **2021**, *878*, 160267. <https://doi.org/10.1016/j.jallcom.2021.160267>.
- (5) Snow, C. S.; Brewer, L. N.; Gelles, D. S.; Rodriguez, M. A.; Kotula, P. G.; Banks, J. C.; Mangan, M. A.; Browning, J. F. Helium Release and Microstructural Changes in

- Er(D,T)<sub>2</sub>-x<sub>3</sub>Hex Films. *J. Nucl. Mater.* **2008**, 374 (1), 147–157. <https://doi.org/10.1016/j.jnucmat.2007.07.021>.
- (6) Garcia, P.; Gilibert, E.; Martin, G.; Carlot, G.; Sabathier, C.; Sauvage, T.; Desgardin, P.; Barthe, M.-F. Helium Behaviour in UO<sub>2</sub> through Low Fluence Ion Implantation Studies. *Nucl. Instrum. Methods Phys. Res. Sect. B Beam Interact. Mater. At.* **2014**, 327, 113–116. <https://doi.org/10.1016/j.nimb.2013.11.042>.
- (7) Taverna, D.; Kociak, M.; Stéphan, O.; Fabre, A.; Finot, E.; Décamps, B.; Colliex, C. Probing Physical Properties of Confined Fluids within Individual Nanobubbles. *Phys. Rev. Lett.* **2008**, 100 (3), 035301. <https://doi.org/10.1103/PhysRevLett.100.035301>.
- (8) Klein, M. P.; Jacobs, B. W.; Ong, M. D.; Fares, S. J.; Robinson, D. B.; Stavila, V.; Wagner, G. J.; Arslan, I. Three-Dimensional Pore Evolution of Nanoporous Metal Particles for Energy Storage. *J. Am. Chem. Soc.* **2011**, 133 (24), 9144–9147. <https://doi.org/10.1021/ja200561w>.
- (9) Catarineu, N. R.; Bartelt, N. C.; Sugar, J. D.; Vitale, S. M.; Shanahan, K. L.; Robinson, D. B. Three-Dimensional Maps of Helium Nanobubbles To Probe the Mechanisms of Bubble Nucleation and Growth. *J. Phys. Chem. C* **2019**, 123 (31), 19142–19152. <https://doi.org/10/ggkxzh>.
- (10) Thiébaud, S.; Décamps, B.; Pénisson, J. M.; Limacher, B.; Percheron Guégan, A. TEM Study of the Aging of Palladium-Based Alloys during Tritium Storage. *J. Nucl. Mater.* **2000**, 277 (2), 217–225. [https://doi.org/10.1016/S0022-3115\(99\)00191-9](https://doi.org/10.1016/S0022-3115(99)00191-9).
- (11) Crowther, R. A.; DeRosier, D. J.; Klug, A. The Reconstruction of a Three-Dimensional Structure from Projections and Its Application to Electron Microscopy. *Proc. R. Soc. Lond. Math. Phys. Sci.* **1970**, 317 (1530), 319–340. <https://doi.org/10/b3wt9s>.
- (12) Messaoudi, C.; Boudier, T.; Sorzano, C.; Marco, S. TomoJ: Tomography Software for Three-Dimensional Reconstruction in Transmission Electron Microscopy. *BMC Bioinformatics* **2007**, 8 (1), 288. <https://doi.org/10.1186/1471-2105-8-288>.
- (13) Schindelin, J. *et al.*, Fiji: An Open-Source Platform for Biological-Image Analysis. *Nat. Methods* **2012**, 9 (7), 676–682. <https://doi.org/10/f34d7c>.
- (14) ImageJ, R. W. A Public Domain Java Image Processing Program. *Natl. Inst. Ment. Health Bethesda Md. USA* **2008**.
- (15) 3D Slicer <https://www.slicer.org/> (accessed 2020 -01 -22).
- (16) Ollion, J.; Cochenec, J.; Loll, F.; Escudé, C.; Boudier, T. TANGO: A Generic Tool for High-Throughput 3D Image Analysis for Studying Nuclear Organization. *Bioinformatics* **2013**, 29 (14), 1840–1841. <https://doi.org/10.1093/bioinformatics/btt276>.
- (17) Castle, M.; Keller, J. *Plugin Rolling Ball Background Subtraction*; Mental Health Research Institute University of Michigan, 2007.

## TOC graphic

